



Buoyancy-driven heat transfer enhancement in a two-dimensional enclosure utilizing nanofluids

Khalil Khanafer^{a,b}, Kambiz Vafai^{a,*}, Marilyn Lightstone^b

^a *Mechanical Engineering Department, University of California, A363 Bourns Hall, Riverside, CA 92521-0425, USA*

^b *Mechanical Engineering Department, McMaster University, Hamilton, Canada L8S 4L7*

Received 26 November 2002; received in revised form 8 March 2003

Abstract

Heat transfer enhancement in a two-dimensional enclosure utilizing nanofluids is investigated for various pertinent parameters. A model is developed to analyze heat transfer performance of nanofluids inside an enclosure taking into account the solid particle dispersion. The transport equations are solved numerically using the finite-volume approach along with the alternating direct implicit procedure. Comparisons with previously published work on the basis of special cases are performed and found to be in excellent agreement. The effect of suspended ultrafine metallic nanoparticles on the fluid flow and heat transfer processes within the enclosure is analyzed and effective thermal conductivity enhancement maps are developed for various controlling parameters. In addition, an analysis of variants based on the thermophysical properties of nanofluid is developed and presented. It is shown that the variances within different models have substantial effects on the results. Finally, a heat transfer correlation of the average Nusselt number for various Grashof numbers and volume fractions is presented.

© 2003 Elsevier Ltd. All rights reserved.

1. Introduction

Nanotechnology is considered by many to be one of the significant forces that drive the next major industrial revolution of this century. It represents the most relevant technological cutting edge currently being explored. It aims at manipulating the structure of the matter at the molecular level with the goal for innovation in virtually every industry and public endeavor including biological sciences, physical sciences, electronics cooling, transportation, the environment and national security.

Low thermal conductivity of conventional heat transfer fluids such as water, oil, and ethylene glycol mixture is a primary limitation in enhancing the performance and the compactness of many engineering electronic devices. To overcome this drawback, there is a strong motivation to develop advanced heat transfer

fluids with substantially higher conductivities to enhance thermal characteristics. Small particles (nanoparticles) stay suspended much longer than larger particles. If particles settle rapidly (microparticles), more particles need to be added to replace the settled particles, resulting in extra cost and degradation in the heat transfer enhancement. As such an innovative way in improving thermal conductivities of a fluid is to suspend metallic nanoparticles within it. The resulting mixture referred to as a nanofluid possesses a substantially larger thermal conductivity compared to that of traditional fluids [1].

The presence of the nanoparticles in the fluids increases appreciably the effective thermal conductivity of the fluid and consequently enhances the heat transfer characteristics. Nanofluids have a distinctive characteristic, which is quite different from those of traditional solid–liquid mixtures in which millimeter and/or micrometer-sized particles are involved. Such particles can clot equipment and can increase pressure drop due to settling effects. Moreover, they settle rapidly, creating substantial additional pressure drop. However, nanofluids exhibit little or no penalty in pressure drop when

* Corresponding author. Tel.: +1-909-787-2135; fax: +1-909-787-2899.

E-mail address: vafai@engr.ucr.edu (K. Vafai).

oped an expression for the effective thermal conductivity of two-component mixtures as a function of liquid and solid particle thermal conductivities, particle volume fraction, and an empirical scaling factor that takes into account the effect of different particle shapes on the effective thermal conductivity. Solid particles suffer from significant clogging problems due to their significant size conductivity. An alternative expression for calculating the effective thermal conductivity of solid–liquid mixtures with a sphericity of one was established by Wasp [11].

Two main approaches have been adopted in the literature to investigate the heat transfer enhancement by small solid particles (millimeter and/or micrometer-sized particles) suspended in a fluid. The first approach is the two-phase model, which enables a better understanding of both the fluid and the solid phases role in the heat transfer process. The second approach is the single-phase model in which both the fluid phase and the particles are in thermal equilibrium state and flow with the same local velocity. The latter approach is simpler and more computationally efficient. Several factors may affect heat transfer enhancement using nanofluids. These factors include gravity, Brownian motion, layering at the solid/liquid interface, ballistic phonon transport through the particles, nanoparticles clustering, and the friction between the fluid and the solid particles. The phenomena of Brownian diffusion, sedimentation, and dispersion may coexist in the main flow of a nanofluid. In the absence of any experimental data and suitable theoretical studies in the literature to investigate these factors, the existing macroscopic two-phase model is not applicable for analyzing nanofluids. Accordingly the modified single-phase, taking into the account some of the above factors, is more convenient than the two-phase model if the main interest is focused on the heat transfer process. Moreover, superior characteristics of the nanofluid allow it to behave more like a fluid than the conventional solid–fluid mixtures.

The chaotic movement of the ultrafine particles increases the energy exchange rates in the fluid, i.e., thermal dispersion takes place within the flow of the nanofluid. To account for the random motion of the particles, dispersion model is implemented. So far, there is a lack of theoretical and experimental works published on the thermal diffusivity coefficients of nanofluids. Thermal diffusivity coefficient for nanofluid can be modeled similar to the thermal dispersion models for flow through porous media. The dispersed model was first applied by Taylor [12] to simulate salt diffusion in water. Xuan and Li [13] presented a procedure for preparing a nanofluid which is a suspension consisting of nanophase powders and a base liquid. Later on, Xuan and Roetzel [14], analyzed theoretically the flow of a nanofluid inside a tube using a dispersion model. Recently, Kebllinski et al. [3] investigated

the mechanisms of heat flow in suspensions of nano-sized particles (nanofluids). Four possible explanations were reported for an increase in the thermal conductivity with decreasing grain size. They developed a fundamental understanding of heat transport in solid nanoparticle colloids under stationary conditions.

To the best knowledge of the authors, the problem of buoyancy-driven heat transfer enhancement of nanofluids in a two-dimensional enclosure has not been analyzed. This problem may be encountered in a number of electronic cooling and MEMS applications. The present study is focused on the analysis of several pertinent parameters on the heat transfer characteristics of nanofluids within the enclosure. The dispersion effect is analyzed in the present investigation. Effective thermal conductivity maps will be developed in the present study for various pertinent parameters.

2. Mathematical formulation

Consider a two-dimensional enclosure of height H and width L filled with a nanofluid as shown in Fig. 1. The horizontal walls are assumed to be insulated, non-conducting, and impermeable to mass transfer. The nanofluid in the enclosure is Newtonian, incompressible, and laminar. The nanoparticles are assumed to have a uniform shape and size. Moreover, it is assumed that both the fluid phase and nanoparticles are in thermal equilibrium state and they flow at the same velocity. The left vertical wall is maintained at a high temperature (T_H) while the right vertical wall is kept at a low temperature (T_L). The thermophysical properties of the nanofluid are assumed to be constant except for the density variation in the buoyancy force, which is based on the Boussinesq approximation.

The initial and boundary conditions for the present investigation are presented as

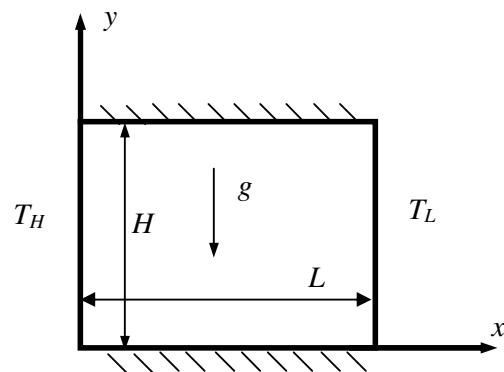


Fig. 1. Schematic for the physical model.

$$u = v = T = 0 \quad \text{for } t = 0 \quad (1)$$

$$\left. \begin{aligned} u = v = \frac{\partial T}{\partial y} = 0 & \quad \text{at } y = 0, H \text{ and } 0 \leq x \leq L \\ T = T_H, \quad u = v = 0 & \quad \text{at } x = 0, \quad 0 \leq y \leq H \\ T = T_L, \quad u = v = 0 & \quad \text{at } x = L, \quad 0 \leq y \leq H \end{aligned} \right\} \quad (2)$$

for $t > 0$

The governing equations for the present study taking into the account the above mentioned assumptions are written in dimensional form as

Vorticity equation

$$\frac{\partial \omega}{\partial t} + u \frac{\partial \omega}{\partial x} + v \frac{\partial \omega}{\partial y} = \frac{\mu_{\text{eff}}}{\rho_{\text{nf},o}} \nabla^2 \omega + \frac{1}{\rho_{\text{nf},o}} [\phi \rho_{s,o} \beta_s + (1 - \phi) \rho_{f,o} \beta_f] g \frac{\partial T}{\partial x} \quad (3)$$

Energy equation

$$\frac{\partial T}{\partial t} + u \frac{\partial T}{\partial x} + v \frac{\partial T}{\partial y} = \frac{\partial}{\partial x} \left[\left(\alpha_{\text{nf}} + \frac{k_d}{(\rho c_p)_{\text{nf}}} \right) \frac{\partial T}{\partial x} \right] + \frac{\partial}{\partial y} \left[\left(\alpha_{\text{nf}} + \frac{k_d}{(\rho c_p)_{\text{nf}}} \right) \frac{\partial T}{\partial y} \right] \quad (4)$$

Kinematics equation

$$\frac{\partial^2 \psi}{\partial x^2} + \frac{\partial^2 \psi}{\partial y^2} = -\omega \quad (5)$$

where $\alpha_{\text{nf}} = (k_{\text{eff}})_{\text{stagnant}} / (\rho c_p)_{\text{nf}}$.

The effective density of a fluid containing suspended particles at a reference temperature is given by

$$\rho_{\text{nf},o} = (1 - \phi) \rho_{f,o} + \phi \rho_{s,o} \quad (6)$$

where $\rho_{f,o}$, $\rho_{s,o}$, and ϕ are the density of clear fluid, density of the particles, and the volume fraction of the nanoparticles, respectively. The effective viscosity of a fluid of viscosity μ_f containing a dilute suspension of small rigid spherical particles is given by Brinkman [15] as

$$\mu_{\text{eff}} = \frac{\mu_f}{(1 - \phi)^{2.5}} \quad (7)$$

The heat capacitance of the nanofluid can be presented as

$$(\rho c_p)_{\text{nf}} = (1 - \phi) (\rho c_p)_f + \phi (\rho c_p)_s \quad (8)$$

The effective stagnant thermal conductivity of the solid-liquid mixture was introduced by Wasp [11] as follows

$$\frac{(k_{\text{eff}})_{\text{stagnant}}}{k_f} = \frac{k_s + 2k_f - 2\phi(k_f - k_s)}{k_s + 2k_f + \phi(k_f - k_s)} \quad (9)$$

This equation is applicable for the two-phase mixture containing micro-sized particles. In the absence of any convenient formula for the calculations of the stagnant thermal conductivity of nanofluids, Eq. (9) may approximately apply to obtain a reasonable estimation.

The effective thermal conductivity of the nanofluid may take the following form

$$k_{\text{eff}} = (k_{\text{eff}})_{\text{stagnant}} + k_d \quad (10)$$

Therefore, the enhancement in the thermal conductivity due to the thermal dispersion is given as [16]

$$k_d = C(\rho c_p)_{\text{nf}} |\bar{V}| \phi d_p \quad (11)$$

where $|\bar{V}| = \sqrt{u^2 + v^2}$ and C is an unknown constant which should be determined by matching experimental data. The above equations can be cast in non-dimensional form by incorporating the following dimensionless parameters

$$\left. \begin{aligned} X = \frac{x}{H}, \quad Y = \frac{y}{H}, \quad U = \frac{u}{\sqrt{g \beta_f \Delta T H^3}}, \\ V = \frac{v}{\sqrt{g \beta_f \Delta T H^3}}, \quad \tau = \frac{t \sqrt{g \beta_f \Delta T H^3}}{H}, \quad \Omega = \frac{\omega H}{\sqrt{g \beta_f \Delta T H^3}}, \\ \Psi = \frac{\psi}{H \sqrt{g \beta_f \Delta T H^3}}, \quad \theta = \frac{T - T_L}{T_H - T_L}, \end{aligned} \right\} \quad (12)$$

$$\frac{\partial \Omega}{\partial \tau} + U \frac{\partial \Omega}{\partial X} + V \frac{\partial \Omega}{\partial Y} = \frac{\nabla^2 \Omega}{(1 - \phi)^{2.5} \left[\phi \frac{\rho_{s,o}}{\rho_{f,o}} + (1 - \phi) \right] \sqrt{Gr}} + \lambda \frac{\partial \theta}{\partial X} \quad (13)$$

$$\frac{\partial \theta}{\partial \tau} + U \frac{\partial \theta}{\partial X} + V \frac{\partial \theta}{\partial Y} = \frac{1}{Pr \sqrt{Gr}} \left[\frac{\partial}{\partial X} \left(\chi \frac{\partial \theta}{\partial X} \right) + \frac{\partial}{\partial Y} \left(\chi \frac{\partial \theta}{\partial Y} \right) \right] \quad (14)$$

$$\frac{\partial^2 \Psi}{\partial X^2} + \frac{\partial^2 \Psi}{\partial Y^2} = -\Omega \quad (15)$$

where

$$\chi = \frac{\left[\frac{(k_{\text{eff}})_{\text{stagnant}}}{k_f} \right]}{(1 - \phi) + \phi \frac{(\rho c_p)_s}{(\rho c_p)_f}} + C \phi \frac{d_p}{H} Pr \sqrt{Gr} \sqrt{U^2 + V^2} \quad (16)$$

In the above equations, $Gr = g \beta_f \Delta T H^3 / \nu_f^2$ is the Grashof number, $Pr = \nu_f / \alpha_f$ is the Prandtl number and ϕ is the volume fraction of the nanoparticles. The aspect ratio is defined as $A = L/H$ and is assumed unity in this investigation. The diameter of the nanoparticle d_p is taken as 10 nm in the present study. The physical dimension of the enclosure H is chosen to be 1 cm.

The coefficient λ that appears next to the buoyancy term is given as

$$\lambda = \left[\frac{1}{1 + \frac{(1 - \phi) \rho_{f,o}}{\phi \rho_{s,o}}} \frac{\beta_s}{\beta_f} + \frac{1}{1 + \frac{\phi \rho_{s,o}}{(1 - \phi) \rho_{f,o}}} \right] = \frac{\beta_{\text{nf}}}{\beta_f} \quad (17)$$

The Nusselt number of the nanofluids is expected to depend on a number of factors such as thermal conductivity and heat capacitance of both the pure fluid and ultrafine particles, the volume fraction of the suspended

particles, the dimensions of these particles, flow structure, and the viscosity of the nanofluid. The local variation of the Nusselt number of the nanofluid can be expressed as

$$Nu = \frac{Q}{Q_{\text{cond,fluid}}} = -\frac{(k_{\text{eff}})_{\text{stagnant}}}{k_f} \frac{\partial \theta}{\partial X} \quad (18)$$

where

$$Q = -(k_{\text{eff}})_{\text{stagnant}} A \frac{\partial T}{\partial x} \Big|_{x=0}$$

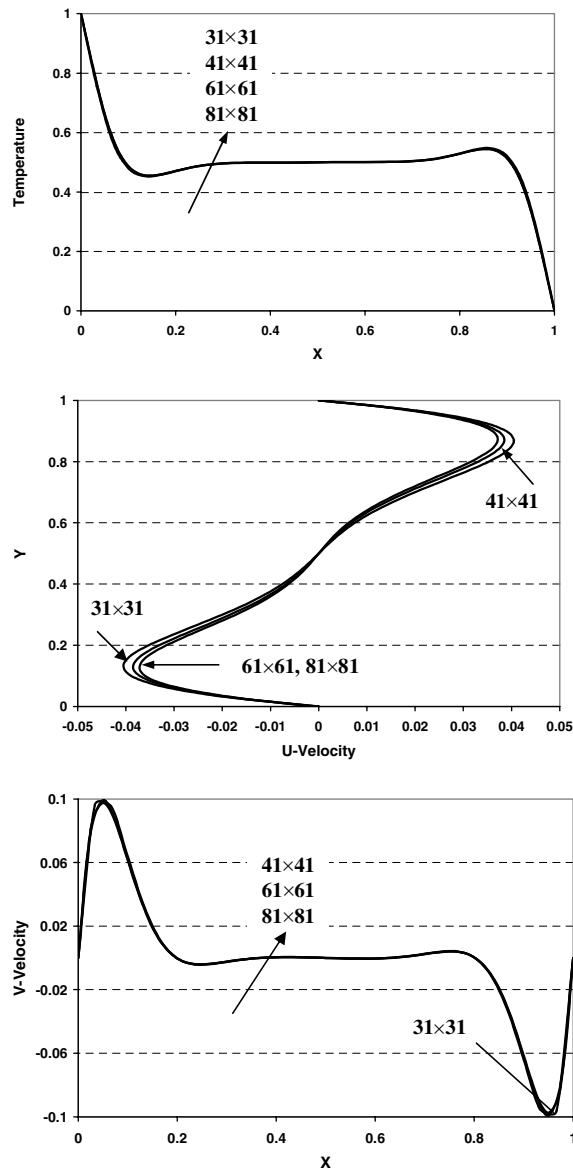


Fig. 2. Velocity and temperature profiles at mid-sections of the cavity for various mesh sizes ($Gr = 10^5$, $Pr = 6.2$, $\phi = 5\%$).

3. Numerical method

The governing equations (13)–(15) were discretized using a finite volume approach [17]. A brief description of the numerical approach is presented here. The governing equations can be represented by a general differential equation as follows

$$\delta_\varphi \frac{\partial \varphi}{\partial \tau} + \frac{\partial}{\partial X} \left[U\varphi - \Gamma_\varphi \frac{\partial \varphi}{\partial X} \right] + \frac{\partial}{\partial Y} \left[V\varphi - \Gamma_\varphi \frac{\partial \varphi}{\partial Y} \right] = S_\varphi \quad (19)$$

where φ stands for either Ω or θ with

$$\delta_\Omega = 1, \quad \Gamma_\Omega = \frac{1}{(1-\phi)^{2.5} \left[\phi \frac{\rho_{s,o}}{\rho_{f,o}} + (1-\phi) \right] \sqrt{Gr}}, \quad S_\Omega = \lambda \frac{\partial \theta}{\partial X} \quad (20)$$

$$\delta_\theta = 1, \quad \Gamma_\theta = \frac{\lambda}{Pr\sqrt{Gr}}, \quad S_\theta = \frac{1}{Pr\sqrt{Gr}} \left(\frac{\partial \chi}{\partial X} \frac{\partial \theta}{\partial X} + \frac{\partial \chi}{\partial Y} \frac{\partial \theta}{\partial Y} \right) \quad (21)$$

The transient finite difference equations, Eqs. (13) and (14), were solved using an alternating direct implicit (ADI) algorithm in conjunction with the power-law

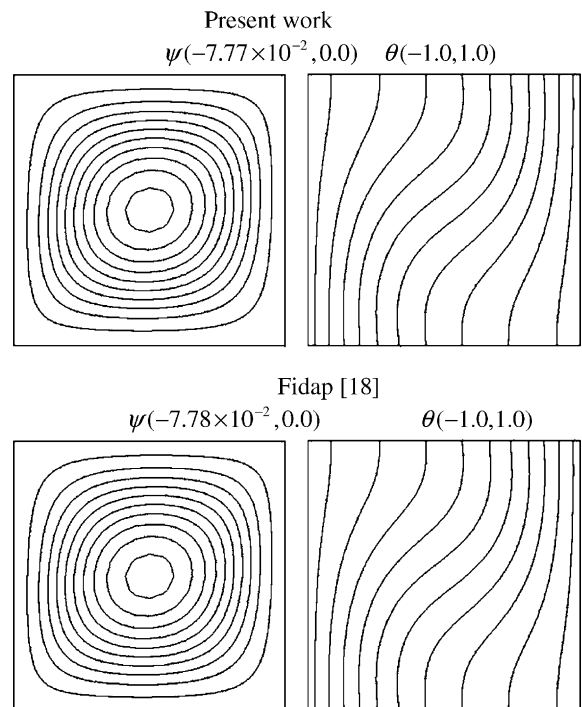


Fig. 3. Comparison of the streamlines and the isotherms between the present work and that of Fidap [18] ($Pr = 0.7$, $Ra = 10^3$).

technique [17]. In addition, false transient accelerator was implemented to expedite the convergence rate of the solution towards steady state condition. Furthermore, successive over relaxation (SOR) method was applied to solve for flow kinematics, as described by Eq. (15).

The vorticity on the boundaries is presented from its definition in terms of the primitive velocity variables as

$$\left. \begin{aligned} \Omega_{i,1} &= \frac{(-4U_{i,2} + U_{i,3})}{2\Delta Y}, & \Omega_{i,N} &= \frac{(4U_{i,N-1} - U_{i,N-2})}{2\Delta Y} \\ \Omega_{1,j} &= \frac{(4V_{2,j} - V_{3,j})}{2\Delta X}, & \Omega_{M,j} &= \frac{(-4V_{M-1,j} + V_{M-2,j})}{2\Delta X} \end{aligned} \right\} \quad (22)$$

To test and assess grid independence of the solution scheme, numerical experiments were performed as shown in Fig. 2. These experiments show that an equally spaced grid mesh of 61×61 is adequate to describe the flow and heat and mass transfer processes correctly. Further increase in the number of grid points produced essentially the same results. The validation of our in-house numerical code was performed against the results generated by a commercial package [18] for pure fluid as shown in Figs. 3–6. It can be seen from these figures that the solution of the present numerical code is in excellent agreement with the numerical results from *FIDAP* [18]

for various Rayleigh numbers. Comparison of the solution with previous works for different Rayleigh numbers is shown in Table 1. The comparison is concerned with the average Nusselt number along the hot wall, maximum and minimum velocity values and their corresponding locations. This table shows an excellent agreement between the present results and other benchmark solutions. Moreover, the present numerical code was also validated against the experimental results of Krane and Jessee [23] for natural convection in an enclosure filled with air as shown in Fig. 7. It can be seen from the comparison that both solutions are in a very good agreement.

4. Discussion

The numerical code developed in the present investigation is used to carry out a number of simulations for a wide range of controlling parameters such as Grashof number and the volume fraction of particles. The range of the Grashof number Gr for this investigation is varied between $10^3 \leq Gr \leq 10^5$. The range of the volume fraction ϕ used in this study is varied between $0 \leq \phi \leq 25\%$. The thermophysical properties of fluid and the solid phases are shown in Table 2.

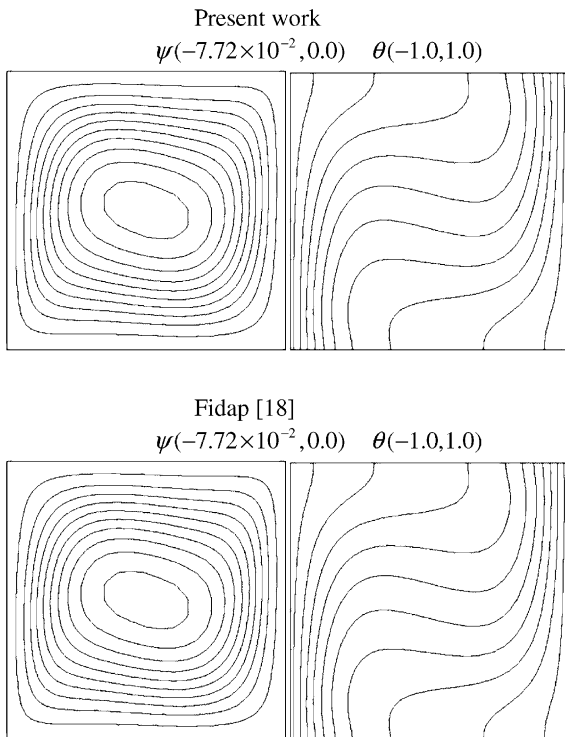


Fig. 4. Comparison of the streamlines and the isotherms between the present work and that of Fidap [18] ($Pr = 0.7$, $Ra = 10^4$).

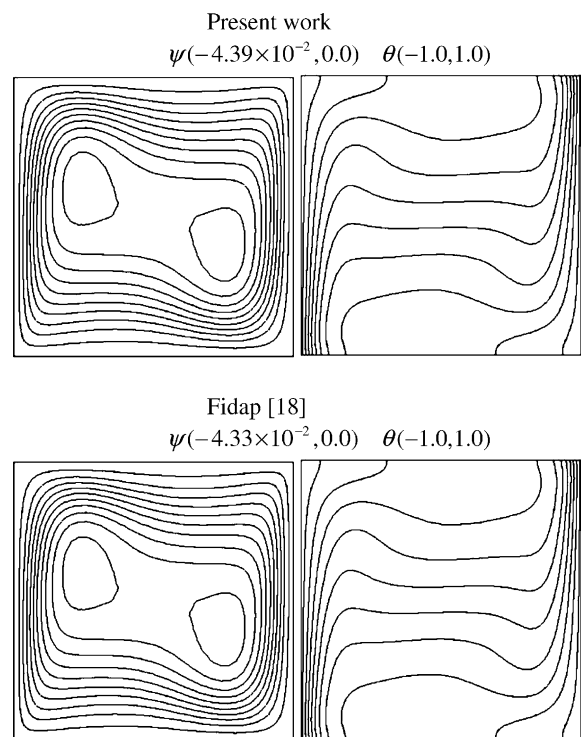


Fig. 5. Comparison of the streamlines and the isotherms between the present work and that of Fidap [18] ($Pr = 0.7$, $Ra = 10^5$).

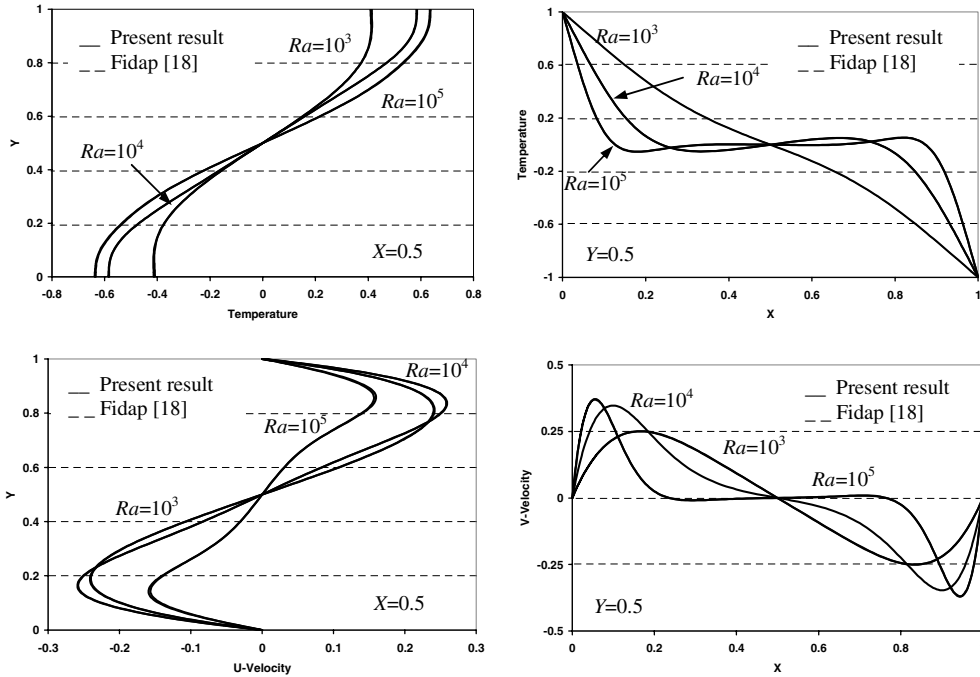


Fig. 6. Comparison of the temperature and velocity profiles at the mid-sections of the cavity between the present results and that of Fidap [18] ($Pr = 0.7$).

Table 1
Comparison of laminar solution with previous works for different Ra -values

	Present	Barakos and Mitsoulis [19]	Markatos and Pericleous [20]	De Vahl Davis [21]	Fusegi et al. [22]
$Ra = 10^3$					
\overline{Nu}	1.118	1.114	1.108	1.118	1.105
U_{max} (at y/H)	0.137 (0.812)	0.153 (0.806)	– (0.832)	0.136 (0.813)	0.132 (0.833)
V_{max} (at x/H)	0.139 (0.173)	0.155 (0.181)	– (0.168)	0.138 (0.178)	0.131 (0.200)
$Ra = 10^4$					
\overline{Nu}	2.245	2.245	2.201	2.243	2.302
U_{max} (at y/H)	0.192 (0.827)	0.193 (0.818)	– (0.832)	0.192 (0.823)	0.201 (0.817)
V_{max} (at x/H)	0.233 (0.123)	0.234 (0.119)	– (0.113)	0.234 (0.119)	0.225 (0.117)
$Ra = 10^5$					
\overline{Nu}	4.522	4.510	4.430	4.519	4.646
U_{max} (at y/H)	0.131 (0.854)	0.132 (0.859)	– (0.857)	0.153 (0.855)	0.147 (0.855)
V_{max} (at x/H)	0.258 (0.065)	0.258 (0.066)	– (0.067)	0.261 (0.066)	0.247 (0.065)
$Ra = 10^6$					
\overline{Nu}	8.826	8.806	8.754	8.799	9.012
U_{max} (at y/H)	0.077 (0.854)	0.077 (0.859)	– (0.872)	0.079 (0.850)	0.084 (0.856)
V_{max} (at x/H)	0.262 (0.039)	0.262 (0.039)	– (0.038)	0.262 (0.038)	0.259 (0.033)

To show that nanofluids behave more like a fluid than the conventional solid–fluid mixture, a comparison of the temperature and the velocity profiles is conducted inside a thermal cavity with isothermal vertical walls at

various Grashof numbers and volume fractions as shown in Fig. 8. This figure shows that the nanofluid behaves more like a fluid than the conventional solid–fluid mixtures in which relatively larger particles with

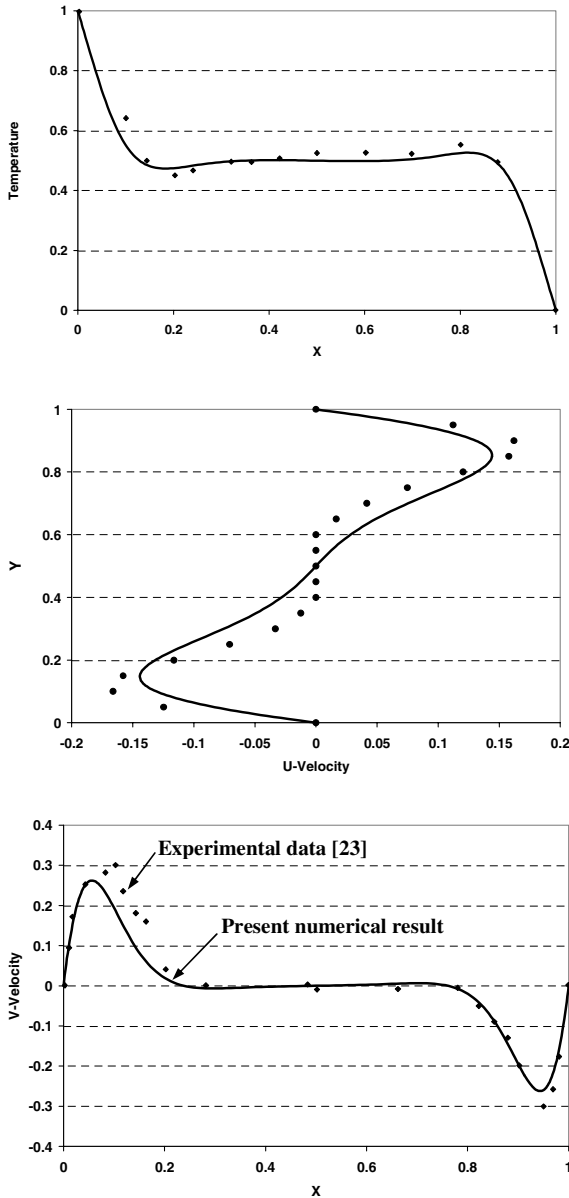


Fig. 7. Comparison of the temperature and the velocity profiles inside a thermal cavity with isothermal vertical walls between the present results and the experimental results by Krane and Jessee [23] ($Ra = 1.89 \times 10^5$, $Pr = 0.71$).

Table 2
Thermophysical properties of different phases

Property	Fluid phase (water)	Solid phase (copper)
c_p (J/kg K)	4179	383
ρ (kg/m ³)	997.1	8954
k (W/m K)	0.6	400
β (K ⁻¹)	2.1×10^{-4}	1.67×10^{-5}

millimeter or micrometer orders are suspended for various Grashof number. Fig. 8 illustrates the effect of Grashof number and the volume fraction on the temperature and the velocity profiles at the mid-sections of the cavity for water with a Prandtl number of 6.2. The numerical results of the present study indicate that the heat transfer feature of a nanofluid increases remarkably with the volume fraction of nanoparticles. As the volume fraction increases, irregular and random movements of particles increases energy exchange rates in the

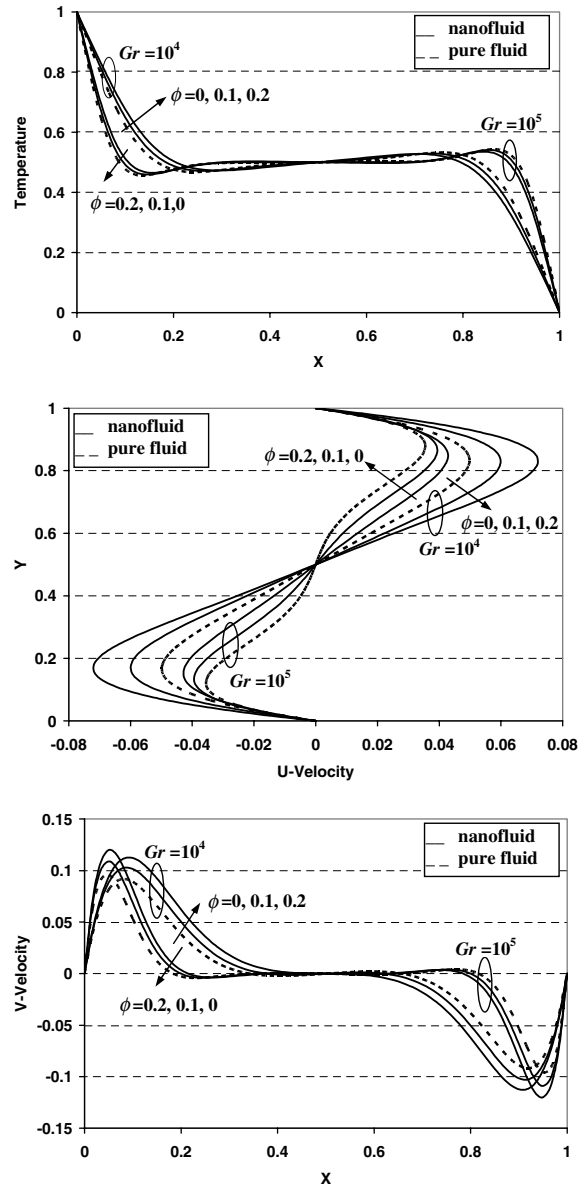


Fig. 8. Comparison of the temperature and velocity profiles between nanofluid and pure fluid for various Grashof numbers ($Pr = 6.2$, $\phi = 10\%$ and 20%).

fluid and consequently enhances the thermal dispersion in the flow of nanofluid. In addition, the velocities at the center of the cavity for higher values of Grashof number are very small compared with those at the boundaries where the fluid is moving at higher velocities. This be-

havior is also present for a single-phase flow. As the volume fraction increases, the velocity components of nanofluid increase as a result of an increase in the energy transport through the fluid. High velocity peaks of the vertical velocity component are shown in this figure at

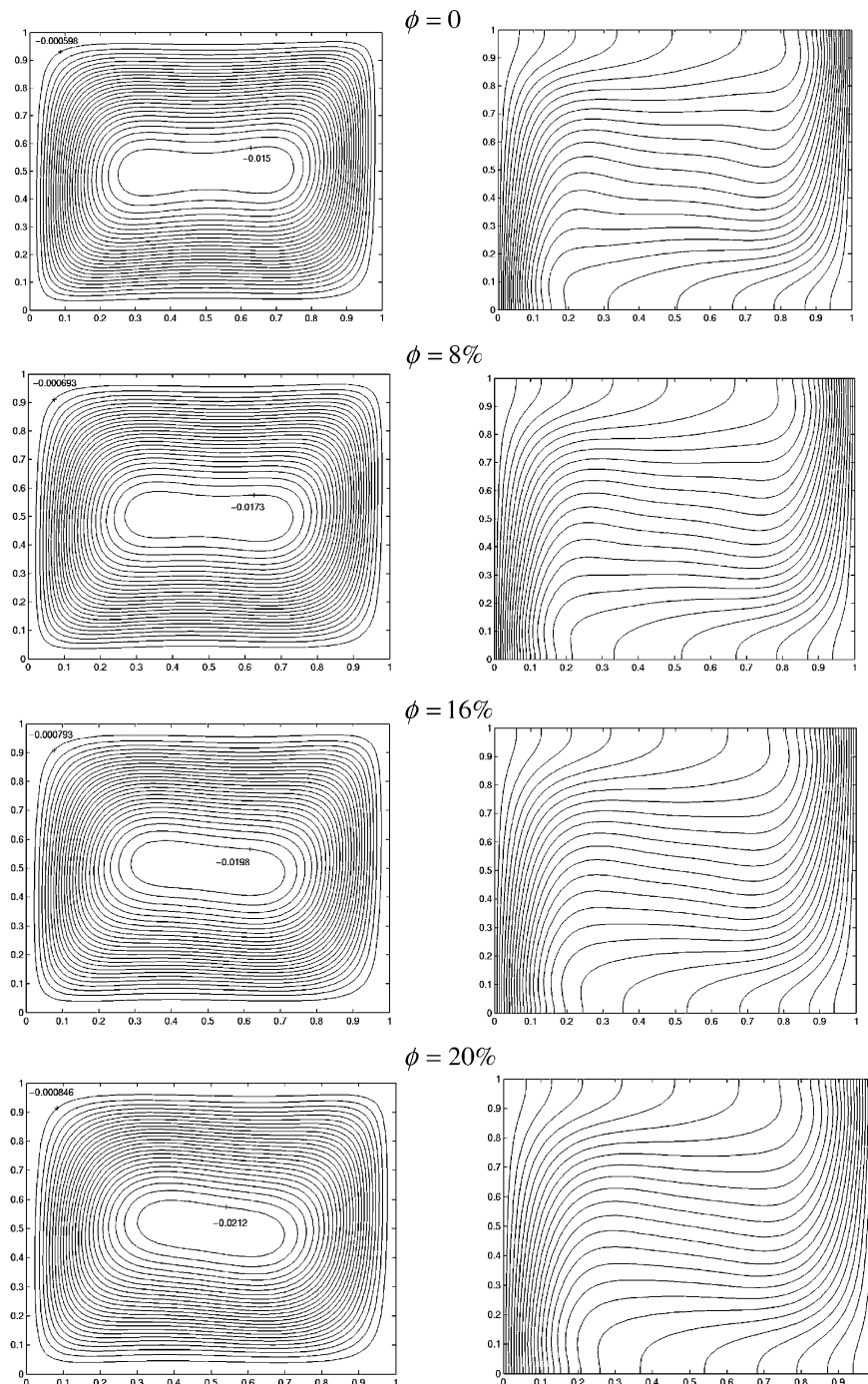


Fig. 9. Streamlines contours and isotherms at various void fractions ($Gr = 10^4$, $Pr = 6.2$).

high volume fractions. The effect of an increase in the volume fraction on the velocity and temperature gradients along the centerline of the cavity is shown in Fig. 8.

The effect of the volume fraction on the streamlines and isotherms of nanofluid for various Grashof numbers is shown in Figs. 9 and 10. In the absence of nanopar-

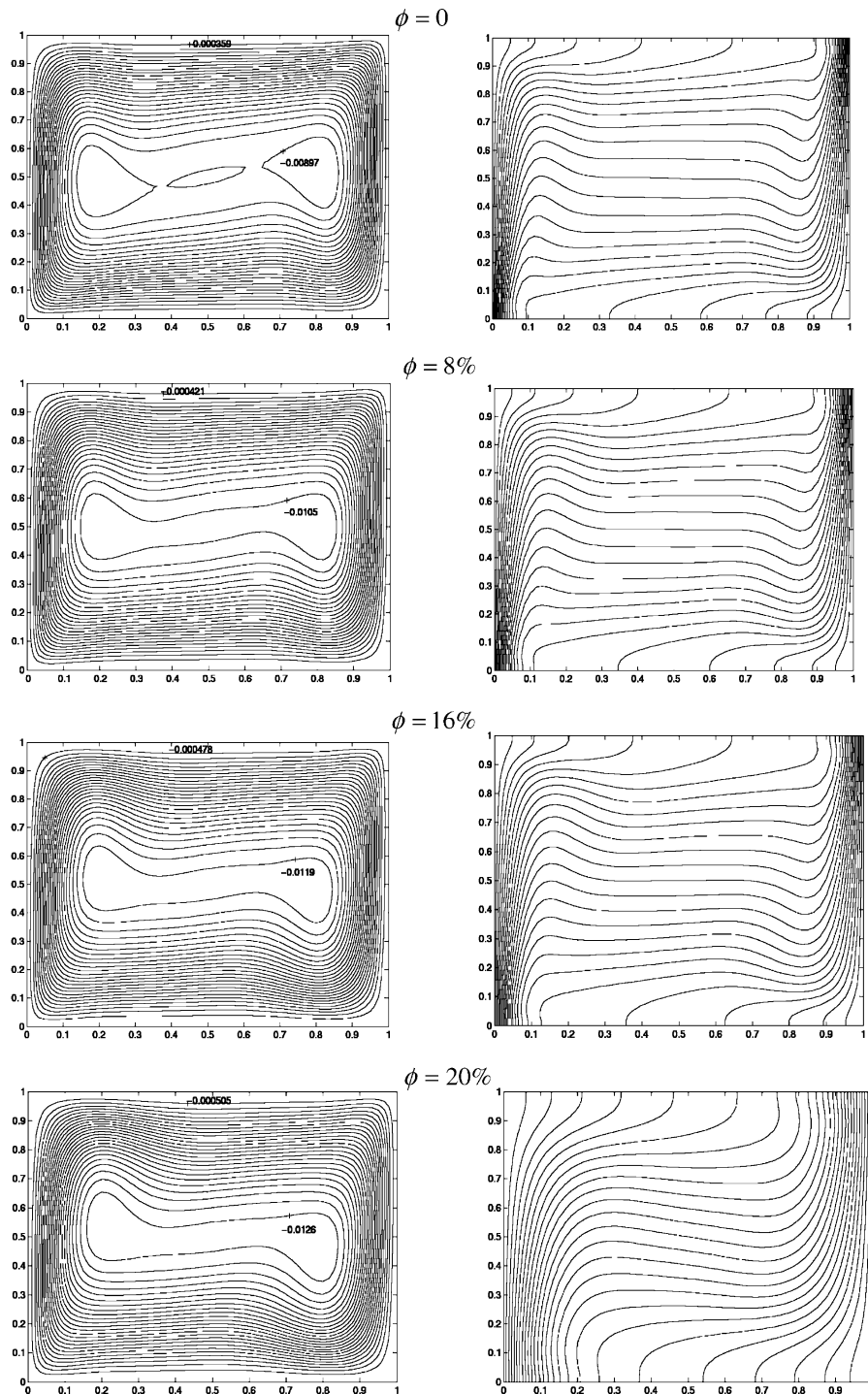
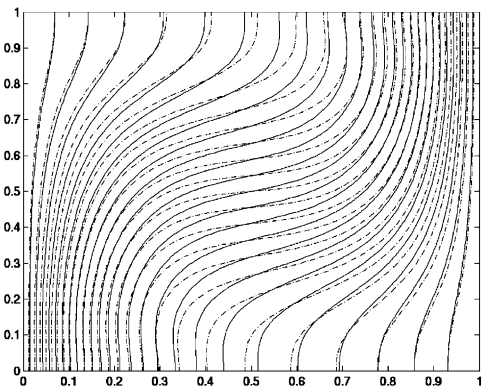
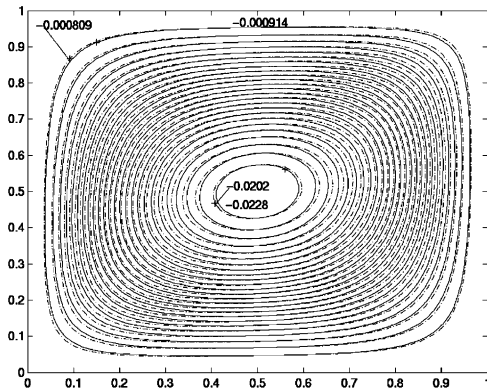


Fig. 10. Streamlines contours and isotherms at various void fractions ($Gr = 10^5$, $Pr = 6.2$).

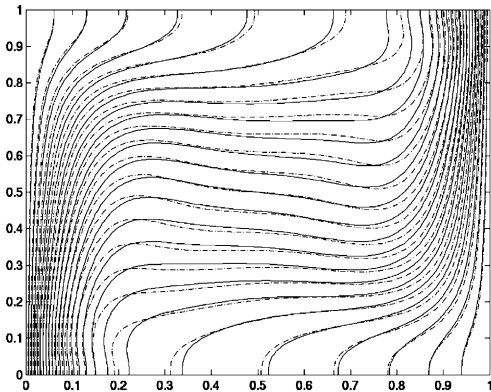
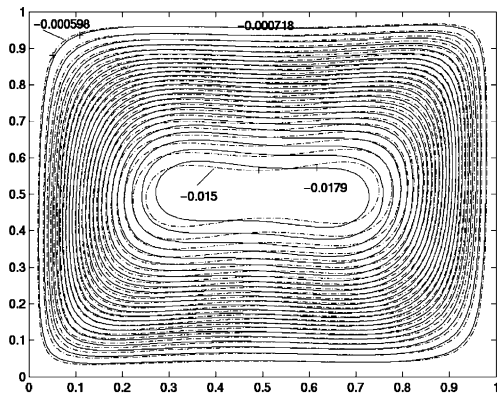
titles and for a low Grashof number ($Gr = 10^3$), a central vortex appears as a dominant characteristic of

the fluid flow. As the Grashof number increases, as shown in Figs. 9 and 10 ($\phi = 0$), the central vortex tends

$Gr = 10^3$



$Gr = 10^4$



$Gr = 10^5$

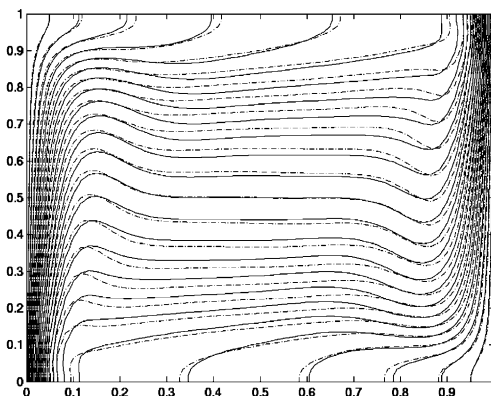
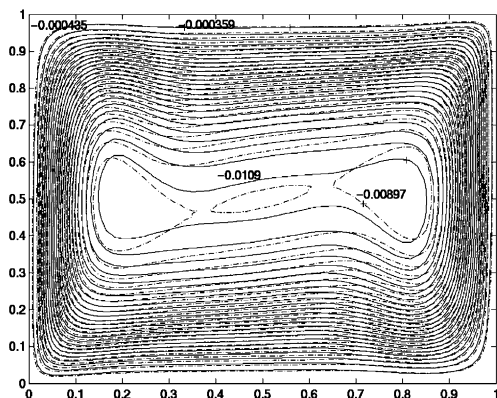


Fig. 11. Comparison of the streamlines and isotherms contours between nanofluid (—) and pure fluid (---) at various Grashof numbers ($\phi = 10\%$).

to become elliptic for $Gr = 10^4$ and eventually breaks up into three vortices for a Grashof number of $Gr = 10^5$. Figs. 9 and 10 show that the intensity of the streamlines

increase with an increase in the volume fraction as a result of high-energy transport through the flow associated with the irregular motion of the ultrafine particles.

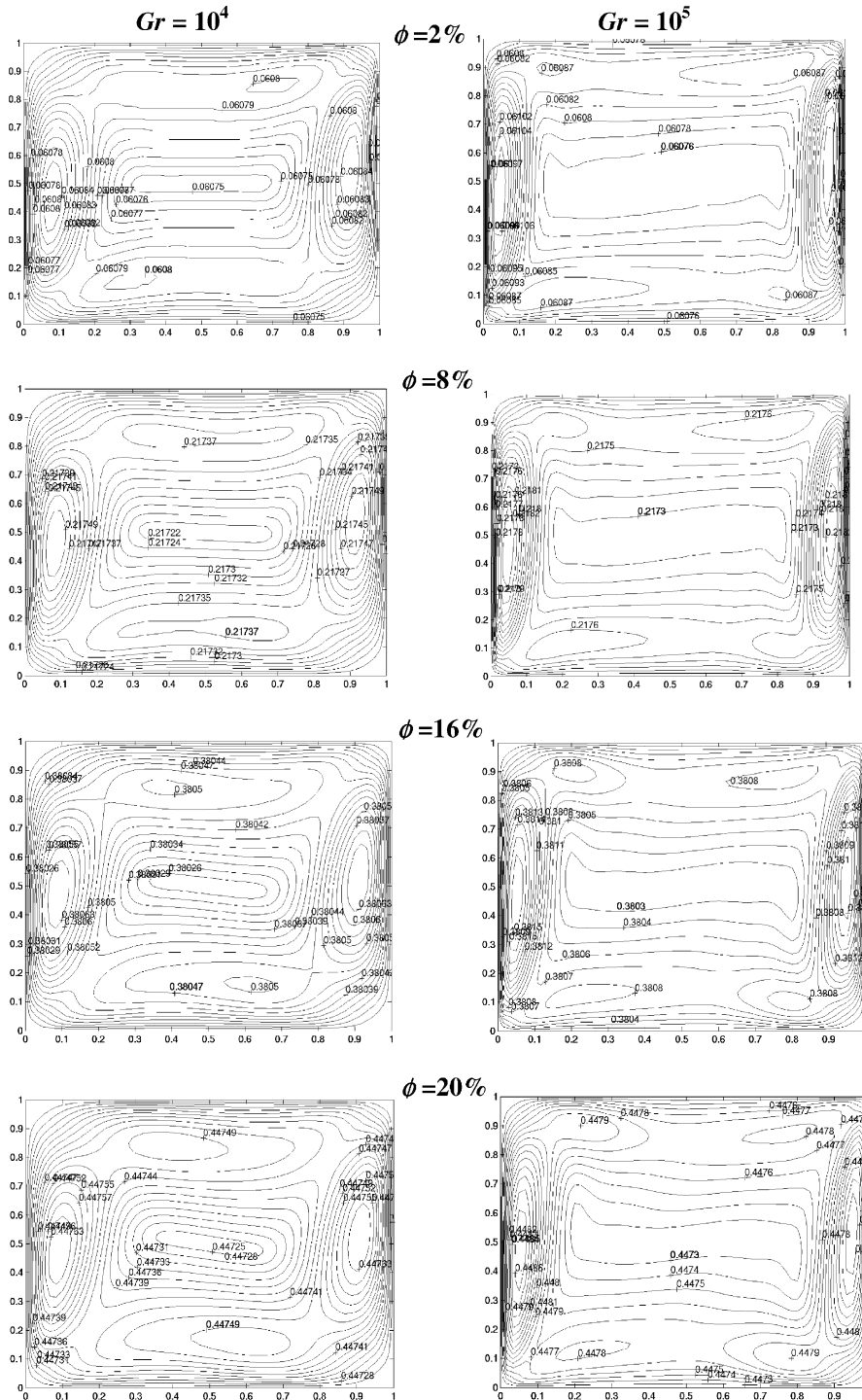


Fig. 12. Effective thermal conductivity enhancement contours ($\times 10^{-2}$) for various volume fractions ($Pr = 6.2$).

In addition, for a Grashof number of 10^4 , the central elliptic vortex of the streamline rotates clockwise as the volume fraction increases. This is associated with higher velocities along the centerline of the enclosure.

As the volume fraction increases, the velocities at the center of the cavity increase as a result of higher solid–fluid transportation of heat. Moreover, the velocities along the vertical walls of the cavity show a higher level of activity as predicted by thin hydrodynamic boundary layers. This is illustrated in the vertical velocity component variation along the horizontal centerline of the cavity for various volume fractions. The isotherms in Figs. 9 and 10 show that the vertical stratification of the isotherms breaks down with an increase in the volume fraction for higher Grashof numbers. This is due to a number of effects such as gravity, Brownian motion, ballistic phonon transport, layering at the solid/liquid interface, clustering of nanoparticles, and dispersion effect. In this study we considered only the effect of dispersion that may coexist in the main flow of a nanofluid.

A comparison of the streamlines and isotherms contours between nanofluid and the conventional fluid is conducted for various Grashof numbers and a volume fraction of $\phi = 10\%$ as shown in Fig. 11. This figure clearly shows the impact of the presence of nanoparticles on the isotherms for a low Grashof number. For a clear fluid, the isotherms at the center of the cavity are horizontal (stratification in the vertical direction) and become vertical only inside the thermal boundary layers at the vertical walls. The streamlines of a clear fluid show that the central vortex occupies a larger zone than that for nanofluid at a Grashof number of 10^4 . For a Grashof number of 10^5 , the central vortex does not breakup into three vortices as in the case of a clear fluid. This is associated with the dispersion effect.

The effective thermal conductivity enhancement contours of the nanofluid within the enclosure at different Grashof numbers and volume fractions are shown in Fig. 12. This figure shows a significant enhancement in the effective thermal conductivity of nanofluid compared to the thermal conductivity of a clear fluid $((k_{\text{eff,nf}} - k_f)/k_f)$.

5. Heat transfer correlation

The average Nusselt number along the hot vertical wall is correlated in terms of the Grashof number ($10^3 \leq Gr \leq 10^5$) and the particles volume fraction ($0 \leq \phi \leq 0.25$). Using the results from the present simulations, the correlation can be expressed as

$$\overline{Nu} = 0.5163(0.4436 + \phi^{1.0809})Gr^{0.3123} \quad (23)$$

where the confidence coefficient of the above equation is determined as $R^2 = 99.9\%$. The average Nusselt number

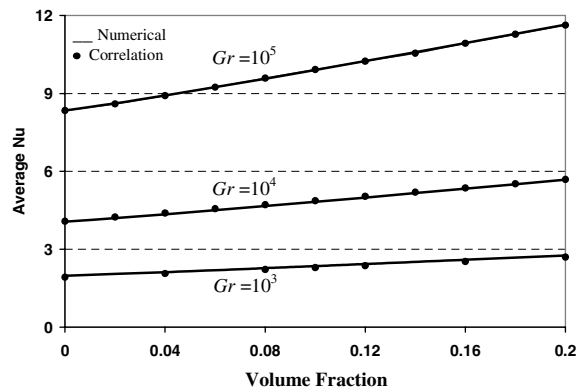


Fig. 13. Comparison of the average Nusselt number between the numerical results and that obtained by the correlation ($Pr = 6.2$).

along the hot wall from the correlation and the numerical results for various Grashof numbers and volume fractions is shown in Fig. 13. This figure shows a linear variation of the average Nusselt number with the void fraction. It should be noted that the trend in Fig. 13 for the average Nusselt number versus the volume fraction would be downward if the Nusselt number is based on the effective thermal conductivity, k_{eff} , instead of the fluid thermal conductivity, k_f . The presence of nanoparticles in the fluid enhances the Nusselt number by about 25% for $Gr = 10^4$ and $Gr = 10^5$ at volume fraction of $\phi = 0.2$. This increase in the average Nusselt number plays a significant role in engineering applications such as in electronic cooling.

6. Sensitivity to model properties

Different models based on the physical properties of nanofluid as displayed in Table 3 are examined with respect to variations of the average Nusselt number as a function of the volume fraction. These variations are based on different scenarios for the density, viscosity, and thermal expansion of nanofluid as shown in Table 2 and displayed in Fig. 14. All models used the effective thermal conductivity of nanoparticles in the present simulations. Fig. 14 gives the upper and lower bounds for the average nanofluid Nusselt number variations for different values of volume fractions. It can be seen that modeling of the density, viscosity and the thermal expansion coefficient of nanofluid play a central role in heat transfer enhancement. Model III has the highest average Nusselt number among other models due to a higher thermal expansion and density, which results in a higher convection heat transfer. It should be noted that model IV has a lower average Nusselt number than model III due to a lower thermal expansion coefficient.

Table 3
Different models of nanofluid density, viscosity, and thermal expansion coefficient

Model	Density	Viscosity	Thermal expansion coefficient	Non-dimensional viscous term	Non-dimensional buoyancy term	Physical basis
I	ρ_f	μ_f	β_f	$\frac{1}{\sqrt{Gr}}$	1	Clear fluid
II	ρ_f	$\mu_{eff} = \frac{\mu_f}{(1-\phi)^{2.5}}$	β_f	$\frac{1}{(1-\phi)^{2.5} \sqrt{Gr}}$	1	$\rho_f \approx \rho_s, \phi \leq 5\%$
III	$\rho_{eff} = \phi\rho_s + (1-\phi)\rho_f$	$\mu_{eff} = \frac{\mu_f}{(1-\phi)^{2.5}}$	β_f	$\frac{1}{(1-\phi)^{2.5} \left[\phi \frac{\rho_{s0}}{\rho_{f0}} + (1-\phi) \right] \sqrt{Gr}}$	1	$\phi \leq 0.5\%$
IV	$\rho_{eff} = \phi\rho_s + (1-\phi)\rho_f$	$\mu_{eff} = \frac{\mu_f}{(1-\phi)^{2.5}}$	$\beta_{eff} = \lambda\beta_f$	$\frac{1}{(1-\phi)^{2.5} \left[\phi \frac{\rho_{s0}}{\rho_{f0}} + (1-\phi) \right] \sqrt{Gr}}$	$\lambda = \left[\frac{1 + \frac{\beta_s}{\beta_f} + \frac{1}{1 + \frac{\rho_{s0}}{\rho_{f0}}}}{1 + \frac{(1-\phi)\rho_{s0}}{\phi\rho_{f0}}} \right]$	General model

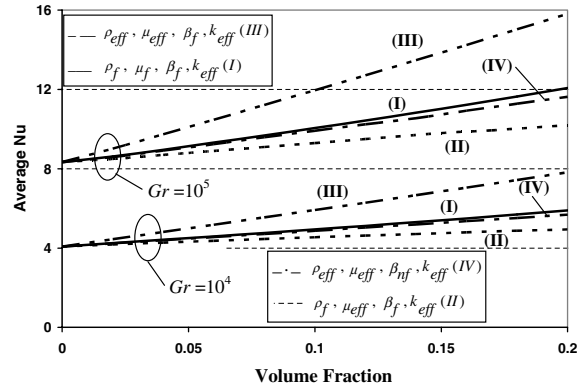


Fig. 14. Average nanofluid Nusselt number variations for different models.

Both models have the same nanofluid density and effective viscosity except for the thermal expansion coefficient which is lower for model IV. As such, the resulting convection heat transfer for model IV is less than the one for model III. Model I has a higher average Nusselt number than model II due to a larger effective viscosity for model II resulting in a thicker momentum boundary layer and an increase in the shear stress between the fluid layers. As such, the average Nusselt number for model II is lower than model I. Models II and III have the same effective viscosity and thermal expansion coefficient except that model III has a higher nanofluid density than model II. Higher effective density indicates higher momentum and consequently more heat transfer enhancement. Model IV is the one that is used as the default model earlier in the paper. It should be noted again that the trend in Fig. 14 for the average Nusselt number versus the volume fraction would be downward if the Nusselt number is based on the effective thermal conductivity, k_{eff} , instead of the fluid thermal conductivity, k_f .

7. Conclusions

Heat transfer enhancement in a two-dimensional enclosure is studied numerically for a range of Grashof numbers and volume fractions. The present results illustrate that the suspended nanoparticles substantially increase the heat transfer rate at any given Grashof number. In addition, the results illustrate that the nanofluid heat transfer rate increases with an increase in the nanoparticles volume fraction. The presence of nanoparticles in the fluid is found to alter the structure of the fluid flow. A comparative study of different models based on the physical properties of nanofluid is analyzed in detail. The variances among these models are analyzed in the present study. The variants among models for the nanofluid density are found to be sub-

stantial. Model III has the highest average Nusselt number. The variants among models for the effective viscosity are found to be more pronounced. Model I is found to have a higher average Nusselt number than model II. Finally, the variants among models for thermal expansion coefficient are found to be significant. A heat transfer correlation for the nanofluid is obtained and verified for various Grashof numbers and volume fractions. This work paves the way for a well-described systematic experimental investigation to better model nanofluids.

Acknowledgements

We acknowledge support of this work by DOD/DARPA/DMEA under grant number DMEA 90-02-2-0216. The grant from National Sciences and Engineering Research Council of Canada (*NSERC-2002*) is acknowledged and appreciated.

References

- [1] J.A. Eastman, S.U.S. Choi, S. Li, W. Yu, L.J. Thompson, Anomalous increase in effective thermal conductivities of ethylene glycol-based nanofluids containing copper nanoparticles, *Appl. Phys. Lett.* 78 (2001) 718–720.
- [2] S.U.S. Choi, Enhancing thermal conductivity of fluids with nanoparticles, in: D.A. Siginer, H.P. Wang (Eds.), *Developments and Applications of Non-Newtonian Flows*, FED-vol. 231/MD-vol. 66, ASME, New York, 1995, pp. 99–105.
- [3] P. Keblinski, S.R. Phillpot, S.U.S. Choi, J.A. Eastman, Mechanisms of heat flow in suspensions of nano-sized particles (nanofluids), *Int. J. Heat Mass Transfer* 45 (2002) 855–863.
- [4] X.W. Wang, X.F. Xu, S.U.S. Choi, Thermal conductivity of nanoparticle–fluid mixture, *J. Thermophys. Heat Transfer* 13 (1999) 474–480.
- [5] H.Q. Xie, J.C. Wang, T.G. Xi, Y. Li, F. Ai, Dependence of the thermal conductivity of nanoparticle–fluid mixture on the base fluid, *J. Mater. Sci. Lett.* 21 (2002) 1469–1471.
- [6] Z. Hashin, S. Shtrikman, A variational approach to the theory of the effective magnetic permeability of multiphase materials, *J. Appl. Phys.* 33 (1962) 3125–3131.
- [7] R.H. Davis, The effective thermal conductivity of a composite material with spherical inclusion, *Int. J. Thermophys.* 7 (1986) 609–620.
- [8] D.J. Jeffrey, Conduction through a random suspensions of spheres, *Proc. R. Soc. Lond. A* 335c (1973) 355–367.
- [9] J.C. Maxwell, *A Treatise on Electricity and Magnetism*, second ed., Oxford University Press, Cambridge, 1904, pp. 435–441.
- [10] R.L. Hamilton, O.K. Crosser, Thermal conductivity of heterogeneous two-component systems, I & EC Fundam. 1 (1962) 182–191.
- [11] F.J. Wasp, *Solid–liquid slurry pipeline transportation*, Trans. Tech. Berlin, 1977.
- [12] G.I. Taylor, Dispersion of soluble matter in solvent flowing through a tube, *Proc. R. Soc. Col. A* 219 (1953) 186–203.
- [13] Y. Xuan, Q. Li, Heat transfer enhancement of nanofluids, *Int. J. Heat Fluid Flow* 21 (2000) 58–64.
- [14] Y. Xuan, W. Roetzel, Conceptions for heat transfer correlation of nanofluids, *Int. J. Heat Mass Transfer* 43 (2000) 3701–3707.
- [15] H.C. Brinkman, The viscosity of concentrated suspensions and solutions, *J. Chem. Phys.* 20 (1952) 571–581.
- [16] A. Amiri, K. Vafai, Analysis of dispersion effects and non-thermal equilibrium, non-Darcian, variable porosity, incompressible flow through porous media, *Int. J. Heat Mass Transfer* 37 (1994) 939–954.
- [17] S.V. Patankar, *Numerical Heat Transfer and Fluid Flow*, Hemisphere, Washington, DC, 1980.
- [18] FIDAP Theoretical Manual, Fluid Dynamics International, Evanston, IL, 1990.
- [19] G. Barakos, E. Mitsoulis, Natural convection flow in a square cavity revisited: laminar and turbulent models with wall functions, *Int. J. Numer. Methods Fluids* 18 (1994) 695–719.
- [20] N.C. Markatos, K.A. Pericleous, Laminar and turbulent natural convection in an enclosed cavity, *Int. J. Heat Mass Transfer* 27 (1984) 772–775.
- [21] G. De Vahl Davis, Natural convection of air in a square cavity, a benchmark numerical solution, *Int. J. Numer. Methods Fluids* 3 (1962) 249–264.
- [22] T. Fusegi, J.M. Hyun, K. Kuwahara, B. Farouk, A numerical study of three-dimensional natural convection in a differentially heated cubical enclosure, *Int. J. Heat Mass Transfer* 34 (1991) 1543–1557.
- [23] R.J. Krane, J. Jessee, Some detailed field measurements for a natural convection flow in a vertical square enclosure, *Proceedings of the First ASME-JSME Thermal Engineering Joint Conference*, vol. 1, 1983, pp. 323–329.